ACS OMEGA

Open Access

http://pubs.acs.org/journal/acsodf

Article

Microwave Construction of NiSb/NiTe Composites on Ni-Foam for High-Performance Supercapacitors

Haidong Zhao, Xiaoyan Hu, Hongjie Kang, Feng Feng,* Yong Guo,* and Zhen Lu*

Cite This: *ACS Omega* 2024, 9, 2597−2605

Read Online

ACCESS | Metrics & More | Article Recommendations | Supporting Information

ABSTRACT: In this paper, NiSb/NiTe/Ni composites were smoothly developed via the microwave method for supercapacitors. The synthesis of NiSb/NiTe crystals was revealed by X-ray photoelectron spectroscopy and X-ray diffraction. The analytic results of scanning electron microscopy and energy dispersive spectroscopy uncover the microscopic morphology as well as the constituent elements of the composites. Self-supported NiSb/NiTe is a supercapacitor cathode that combines high capacitance with excellent cycling stability. The obtained composite electrode displayed remarkable electrochemical properties, presenting a special capacitance of 1870 F g^{-1} (1 A g^{-1}) and 81.5% of the original capacity through 30,000 times (10 A g^{-1}) of the charging/discharging process. Further, an asymmetric supercapacitor was prepared employing NiSb/NiTe as a cathode and activated carbon as an anode. NiSb/NiTe//AC exhibited a high energy density of 224.6 uW h cm^{-2} with a power density of 750 μW cm^{-2} and provided a favorable cycling stability of 83% after 10,000 cycles.

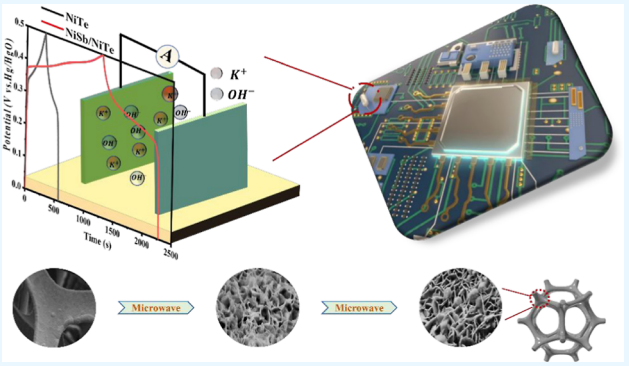

1. INTRODUCTION

Spurred on by the speedy consumption of fossil fuels, the evolution of substitute nonrenewable energy storage and switching devices with sodium-ion batteries (SIBs), fuel cells, and supercapacitors (SCs) has been identified as a means of supplying a sustainable and secure energy source.[1−4] SCs are being used as energy devices for future use owing to their higher power density, excellent cycling stability, and fast charging/discharging characteristics.[5,6]

Among the various electrode materials, Ni-based sulfides such as NiS,[7,8] NiSe,[9] and NiTe[10] are extensively utilized as electrode materials in SCs for their high theoretical capacitance, remarkable redox properties, and low cost.[11−13] Compared to NiS and NiSe, NiTe has higher electrical conductivity and an easily tunable electronic structure as well as proven good pseudocapacitance characteristics and excellent cycling stability.[14,15] For instance, Ye et al.[16] demonstrated that the capacitance value of NiTe is 109.4 mA h g^{-1}, resulting in a capacity maintenance rate of 98% after 5000 cycles. M. Manikandan et al.[17] synthesized a NiTe nanorod electrode by a hydrothermal method, possessing 618 F g^{-1}, and the capacitance was able to maintain 75% of it through 5000 cycles. Nevertheless, the capacitance value of NiTe is very low and not sufficient for SC applications.[18] Compounding is an effective method of modulating the electron structure to provide additional redox reactions.[19−21] Antimony metal shows superior electrochemical performance in the application of energy storage thanks to its good electrical conductivity (1.6 × 10^4 S m^{-1}), high theoretical capacitance value (660 mA h g^{-1}), and fast ionic diffusion property.[22,23] Composite Sb compounds can tune the overall electrical conductivity and take advantage of the respective capacitive contribution and the synergistic effect of multiple active species, resulting in higher specific capacities.[24−26] For example, Usui et al.[27] prepared CeO_2/Sb_2O_3 composites for sodium storage by mechanical grinding. The CeO_2/Sb_2O_3 composite electrode exhibited 400 mA h g^{-1} capacity during the 120th cycle, greatly improving the capacity compared to the low capacity of CeO_2 (25 mA h g^{-1}) during the first charge/discharge process. Jia et al.[28] synthesized $Sb_2S_3/SnS_2/C$ electrodes via the solvothermal method, showing a reversible capacity of 642 mA h g^{-1} after 600 cycles. The value of the capacity was severely reduced to 100 mA h g^{-1} (1 A g^{-1}) through 20 cycles relative to the SnS_2/C electrode. Li et al.[29] constructed $CoSe_2/Sb_2Se_3$ anode SIBs by an ion exchange reaction. The $CoSe_2/Sb_2Se_3$ composite electrode exhibited enhanced sodium ion storage capacity compared to that of $CoSe_2$, reaching 512.9 mA h g^{-1} at 0.1 A g^{-1}. Therefore, making full use of the capacitive contribution of both components by introducing antimony-based compounds

Received: September 25, 2023
Revised: December 9, 2023
Accepted: December 13, 2023
Published: December 29, 2023

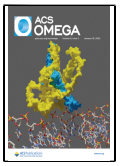

as complexes is an effective strategy to promote multiple redox reactions and increase the capacitance value.

Compared with traditional synthesis methods such as hydrothermal and solvent thermal methods, the microwave method of preparing electrode materials has the merits of short time consumption and environmental conservation.[30−32] Herein, NiSb/NiTe composites self-supported on nickel foam were prepared via microwave radiation. Combining NiSb and NiTe results in increased conductivity, providing more chemical reaction sites and reducing the migration routes of electrons and ions.[33,34] The NiSb/NiTe cathode achieves 1870 F g^{-1} at 1 A g^{-1} and a capacity maintenance of 81.5% through 30,000 cycles. In parallel, the NiSb/NiTe//activated carbon (AC) presents a maximum value of 224.6 uW h cm^{-2} in energy density and a satisfactory cycling stability of 83% after 10,000 cycles.

2. EXPERIMENTAL SECTION

2.1. Materials. Ni-foam (NF) was purchased from LongShengBao Products Corporation. Tellurium powder was sourced from Aladdin Industrial Corporation. $SbCl_3$ was taken from Macklin Corporation. $NiCl_2{\cdot}6H_2O$ was purchased from Shanghai Klamar Co. Ethyl alcohol (C_2H_6O), ethylene glycol ($C_2H_6O_2$), ethylenediamine ($C_2H_8N_2$), and potassium hydroxide (KOH) were acquired from Chemical Products Co. (China, Tianjin).

2.2. Preparation of NiTe/Ni. Prior to use, NF (1 × 1 cm^2) was ultrasonically cleaned in ethyl alcohol. In brief, a quantity of Te powder, 400 μL of KOH (0.8 M), and 1.6 mL of $C_2H_8N_2$ were dissolved by stirring to yield a red wine-colored liquid. The above-mentioned mixture was then shifted to a heat-resistant crucible (10 mL) along with NF. After the reaction was maintained at 1000 W for 150 s in a microwave oven, the NF was cleaned with DI water as well as further dried (80 °C, 10 h). The nanoflakes of NiTe on NF weighed about 0.5 mg.

2.3. Preparation of NiSb/NiTe/Ni. The procedure was as follows: $SbCl_3$ and $NiCl_2{\cdot}6H_2O$ were dissolved in 2 mL of C_2H_6O in a molar ratio of 1:1. 100 μL of the above solution, 600 μL of $C_2H_8N_2$, and 400 μL of $C_2H_6O_2$ were added to the NiTe/Ni electrode sheet prepared in the first step as a substrate for sonication for 20 min, and then the microwave reaction (under different conditions) was carried out. Finally, the composite electrodes prepared with the above steps were cleaned using deionized water and left at 80 °C for 10 h. The weight of NiSb/NiTe embedded in the NF was about 1 mg. Table 1 shows the specific capacitance for NiSb/NiTe materials that were prepared under different conditions.

2.4. Fabrication of the NiSb/NiTe/Ni//AC Asymmetric SC. A NiSb/NiTe/Ni//AC device was assembled using a NiSb/NiTe electrode as the positive electrode and a 1 × 1 cm^2 commercial activated carbon (AC) electrode as the negative electrode and tested in 6 M KOH. The negative electrodes were prepared as follows: AC, ethynyl black, and PVDF were blended into a homogeneous slurry at a mass ratio of 80:10:10. The obtained paste was then coated on 1 cm^2 NF, dried at 100 °C for 10 h, and finally pressed into electrode sheets.

Table 1. Specific Capacitance Values of NiSb/NiTe under Various Reaction Conditions[a]

sample	microwave watts/W	microwave duration/s	capacitance/F g^{-1} (1 A g^{-1})
P1	600	150	1046
P2	1000	150	1236
P3	800	150	1870
T1	800	120	1192
T2	800	180	1650

[a]T: microwave time P: microwave power.

2.5. Characterization. The crystallographic structure of NiSb/NiTe was recognized by X-ray diffraction (XRD) (Rigaku MiniFlex 600). The microstructural features and surface topography of the sample were determined by scanning electron microscopy (SEM) (Gemini 300). Identification of the electronic state and the physical elemental distribution of the sample was performed by X-ray photoelectron spectroscopy (XPS) (PHI-5000 VersaProbe III) and energy dispersive spectroscopy (EDS, Gemini 300).

2.6. Electrochemistry Characterization. In 6 M KOH, the electrochemical characterization of NiSb/NiTe composites was evaluated by cyclic voltammetry (CV), constant current charging/discharging (GCD), and EIS. The Pt sheet was applied as an opposite electrode. The selection of a mercuric oxide electrode was used as a reference electrode (RE). These basic measurement data were carried out on an electrochemical workstation (CHI660E). The cycle stability of the material was checked using the Landt cell test system (CT2001A). The capacitance value was calculated through the underneath equation

$$C_S = I\Delta t/m\Delta V \quad (1)$$

I (A) means the amps, m (g) is the quality of the electroactive material, and Δt (s) denotes the discharge time.

The electrode mass of the SC is regulated by the following equation

$$m^+/m^- = C_s^-\Delta V^-/C_s^+\Delta V^+ \quad (2)$$

where ΔV^+ and ΔV^- are the voltage windows where the positive/negative electrodes are located, and C_s^+ and C_s^- are the capacitive amounts of the positive/negative electrodes, respectively.

The E (W h cm^{-2}) and P (W cm^{-2}) C_A (F cm^{-2}) of the device are taken through calculation equations

$$C_A = I\Delta t/S\Delta V \quad (3)$$

$$E_A = I\int V\,dt/3.6 \times m \quad (4)$$

$$P_A = E/\Delta t \times 3600 \quad (5)$$

where S is 1 cm^2.

3. RESULTS AND DISCUSSION

3.1. Characterization of NiSb/NiTe/Ni. The XRD graph of the NiSb/NiTe composite electrode is shown in Figure 1a. The diffractive peaks at 46.1, 42.9, and 31.1° correlate to (110), (102), and (101) of NiTe (JCPDS no. 38-1393), while the derivative peaks at 31.5, 43.9, and 46.2° are attributed to (101), (102), and (110) of NiSb (JCPDS no. 41-1439). The three peaks 44.5, 51.8, and 76.4° correspond to the cubic phase of Ni substrates (JCPDS no. 04-0850). The XRD graph of the NiSb/NiTe electrode after 30,000 cycles is shown in Figure S3. The XPS spectrum favors the existence of the elements Ni, Sb, and Te. Figure 1b shows that the peaks at 855.4/873.5 eV match the Ni $2p_{3/2}$/Ni $2p_{1/2}$ orbitals, and the peaks at 861.1/

https://doi.org/10.1021/acsomega.3c07385
ACS Omega 2024, 9, 2597−2605

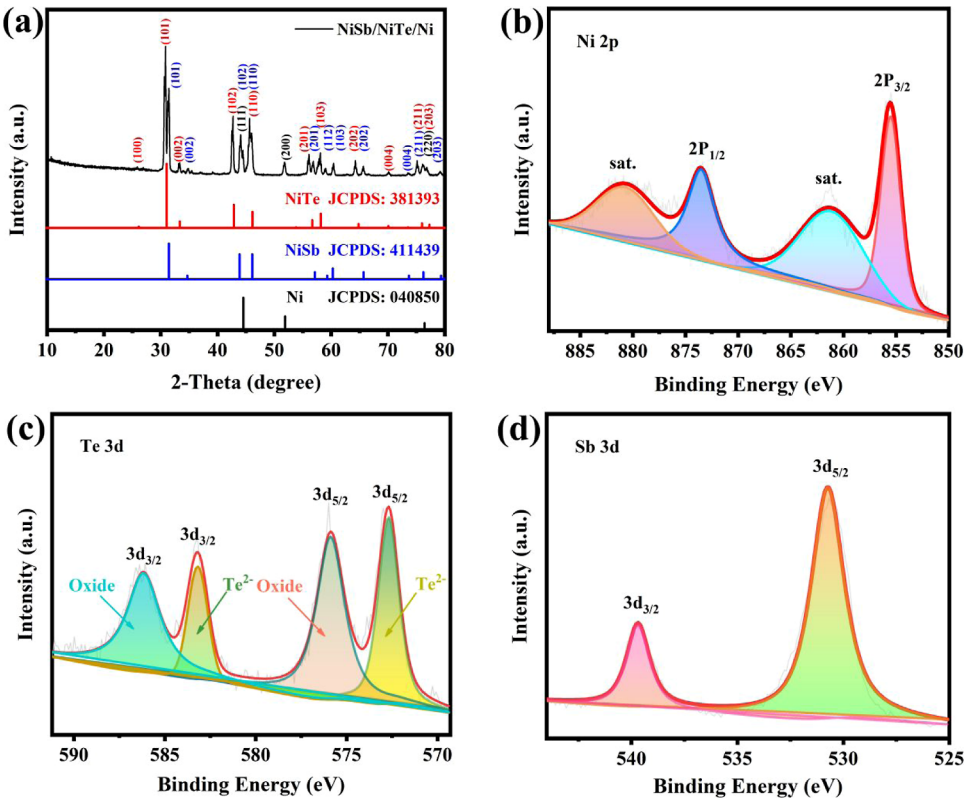

Figure 1. (a) XRD pattern for NiSb/NiTe; XPS pattern of NiSb/NiTe: (b) Ni 2p, (c) Te 3d, and (d) Sb 3d.

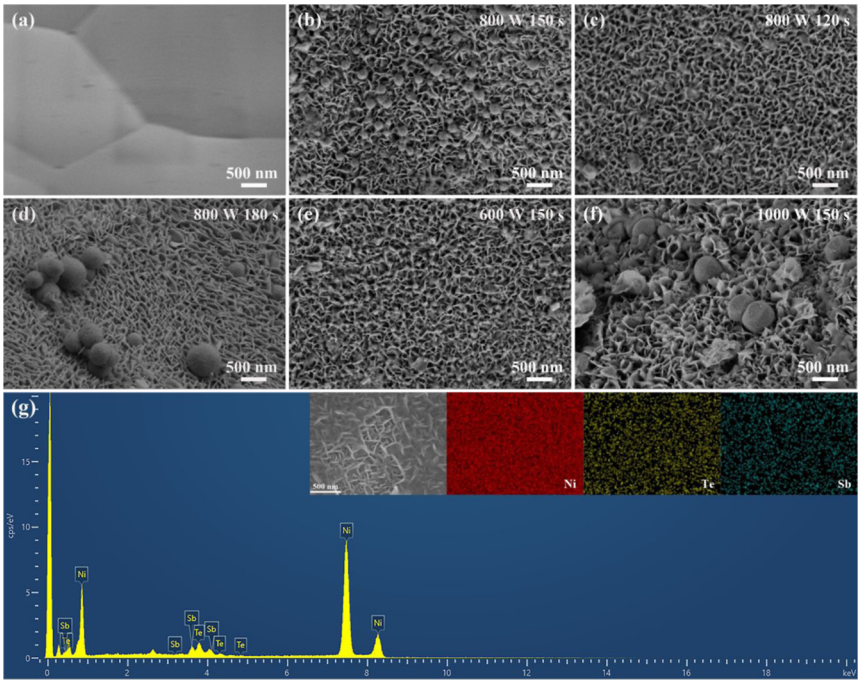

Figure 2. (a) SEM image of NF; (b–f) SEM images of NiSb/NiTe (at various conditions); (g) EDS image of NiSb/NiTe.

880.7 eV are the equivalent for the satellite peaks. The XPS spectrum of Te 3d (Figure 1c) with energetic peaks of about 572.6/583.2 eV is due to Te^{2-}. The other spikes are regarded as the high oxidation state of tellurium due to the oxidation of the surface. The Sb spectrum in Figure 1d has two distinct peaks with combination energies of 539.7 and 530.7 eV, associated with $3d_{3/2}$ and $3d_{5/2}$ of Sb.

Figure 2 shows SEM images of the NiSb/NiTe complexes under different preparation conditions. SEM was used to probe the correlation of the micromorphology with the electrochemical properties of NiSb/NiTe. Under microwave irradiation at 1000 W for 150 s, NiTe was grown uniformly on the surface of nickel foam to form nanosheets. Subsequently, the NiSb alloy particles self-grew on the NiTe sheets, and the

https://doi.org/10.1021/acsomega.3c07385
ACS Omega 2024, 9, 2597−2605

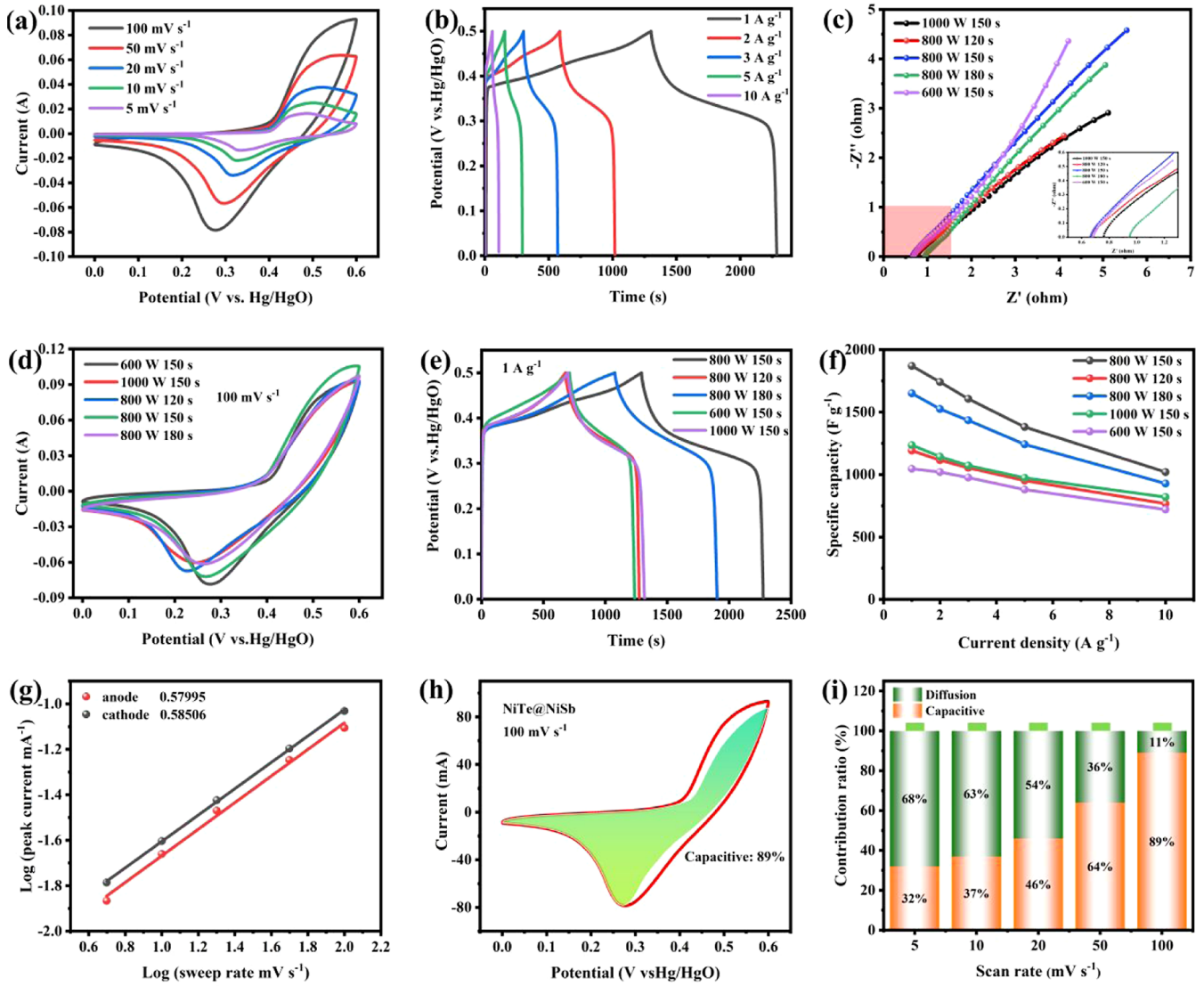

Figure 3. (a) CV profiles of NiSb/NiTe with optimal condition (800 W for 150 s); (b) GCD curves of NiSb/NiTe with sample P3; (c) Nyquist plots for NiSb/NiTe at different reaction parameters; (d) CV profile of NiSb/NiTe at various microwave conditions; (e) GCD profiles of NiSb/NiTe under variable reaction parameters; (f) specific capacity of NiSb/NiTe samples at different current densities under different preparation conditions; (g) calculation of NiSb/NiTe charge storing dynamics; (h) capacitance share of the NiSb/NiTe energy storage at 100 mV s^{-1}; (i) histogram of the contribution of capacitance and diffusion control factor on the total amount of capacity (through varying sweep rates).

overall morphology showed the formation of alloy nanoparticles in the nanosheets. In order to analyze the morphology of the two substances separately, we characterize the morphology of the first layer of NiTe and NiSb/NiTe in Figure S1. In Figure 2b, NiSb is more homogeneously concentrated on the NiTe nanosheets under the optimum reaction conditions (800 W and 150 s). The composite consisting of two species (NiTe and NiSb) possesses more electrochemically active sites to facilitate the redox reaction.[39,40] The capacitance of the NiSb/NiTe/Ni composite electrode is significantly higher compared to that of the self-grown NiTe nanosheets. As shown in Figure 2c, when the microwave exposure time is short, the NiSb particles form less and are inhomogeneous, leading to low electrochemical performance. As shown in Figure 2d, with increasing exposure time, NiSb particles aggregated and eventually became agglomerated in morphology on the NiTe sheet. The capacitance values of the electrode sheets prepared at the two different microwave times mentioned above were significantly lower than those at the optimum conditions, thus showing that microwave time affects the capacitance values of the electrodes. As shown in Figure 2e, the NiSb particles were still inhomogeneous and discontinuous at lower microwave power states. It presents the shape of the specimen after irradiation at 1000 W for 150 s in Figure 2f. For high power, the NiSb particles aggregate and adhere to form aggregates by growing in the voids between the nanosheets, which severely affects the active zone of the electrode. Combining these morphologies suggests that the microstructure of NiSb particles can be modulated by microwave power and time, which directly affects their electrochemical properties.[41,42] In order to further analyze the morphological stability before and after electrochemical cycling, we performed further electron microscopic characterization of the electrodes after electrochemical cycling in Figure S2. EDS combined with Figure 2g shows the successful self-growth of NiSb/NiTe composites on nickel foam. The heterostructure formed by NiSb and NiTe tunes the electronic structure, improves the

https://doi.org/10.1021/acsomega.3c07385
ACS Omega 2024, 9, 2597−2605

Table 2. Comparison of the Electrochemical Properties of NiSb/NiTe vs Other Materials

material	method	specific capacity/F g^{-1} (1A g^{-1})	retention rate (%)	Ref
NiTe nanorods	hydrothermal	618.0	75.0% (5000 circles)	17
NiTe/NiSe	electrodeposition	1868.0	86.2% (5000 circles)	35
Se/NiTe	hydrothermal	998.2	93.2% (1000 circles)	36
Co/NiTe	hydrothermal	1645.6	85.0% (1000 circles)	37
NiTe/$NiCoSe_2$	hydrothermal	2018.2	97.7% (5000 circles)	16
NiSb	microwave	4633.0	80.0% (10,000 circles)	38
NiSb/NiTe	microwave	1870.0	81.5% (30,000 circles)	this work

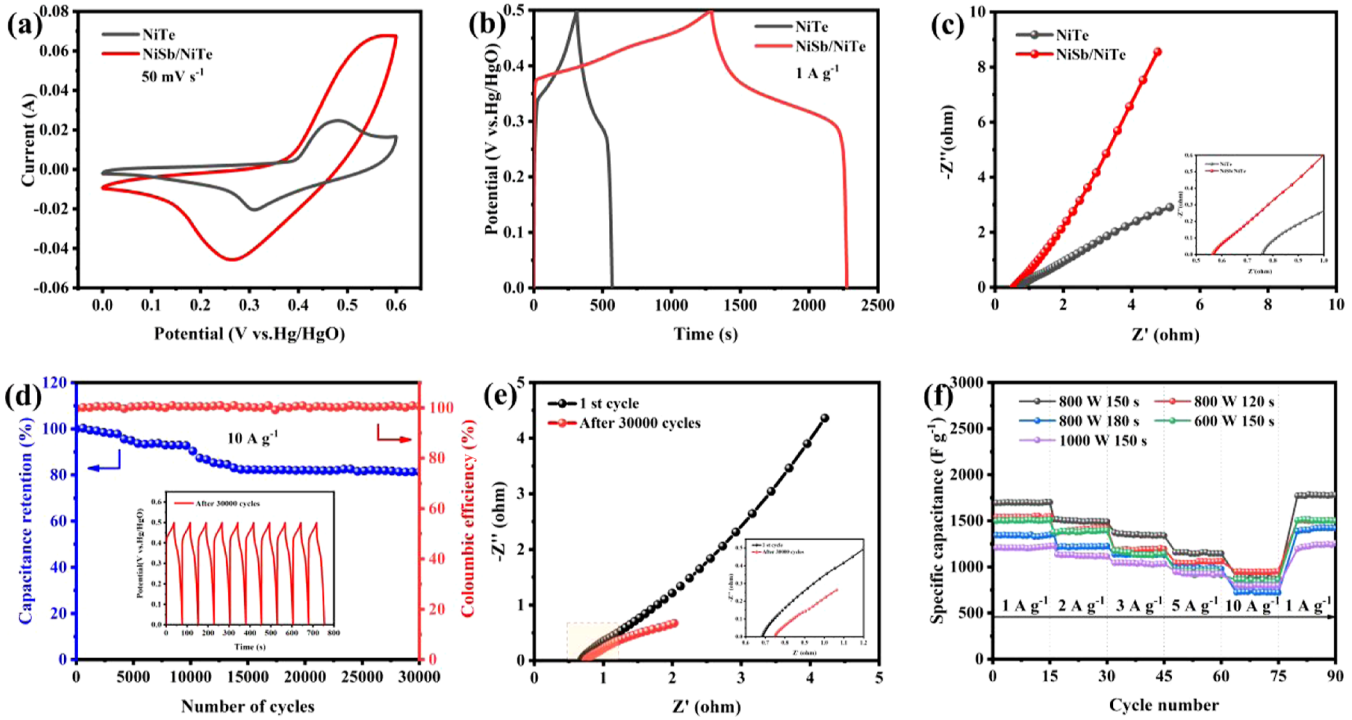

Figure 4. (a) CV plots of NiSb/NiTe and NiTe; (b) GCD profiles of NiSb/NiTe and NiTe at 1 A g^{-1}; (c) resistance plots between NiTe and NiSb/NiTe; (d) degradation of the capacitance of sample P3 in the presence of 30,000 GCDs through 10 A g^{-1}; (e) electrical impedance before and after circulation; (f) rate performance of sample P3.

electrical conductivity, and exposes numerous electrically active sites, which shortens the pathways for electron as well as ion migration.[43−45]

3.2. Electrochemistry Tests. *3.2.1. Electrochemical Properties of NiSb/NiTe/Ni.* Figure 3a presents the CV curves of NiSb/NiTe (800 W, 150 s) in the three-electrode system at various sweeping rates (100, 50, 20, 10, and 5 mV s^{-1}) at a voltage window (0−0.6 V) relative to the Hg/HgO RE. The GCD curves are depicted in Figure 3b, which coincide with the CV curve with two redox peaks in this voltage interval. The NiSb/NiTe electrode has a capacitance of 1870 F g^{-1} through 1 A g^{-1}, based on eq 1. The NiSb/NiTe composite as a SC positive electrode in an alkaline electrolyte lies in a convertible switch reaction with the following reaction mechanism[38,46]

$$NiSb + OH^- \leftrightharpoons Ni(Sb)OH + e^-$$

$$Ni(Sb)OH + 2OH^- \leftrightharpoons Ni(Sb)OOH + H_2O + 2e^-$$

$$NiTe + OH^- \leftrightharpoons NiTeOH + e^-$$

$$NiTeOH + OH^- \leftrightharpoons NiTeO + H_2O + e^-$$

In contrast to other Ni-based electrode materials (listed in Table 2), NiSb/NiTe has a large capacity and excellent circulation stability. As presented in Figure 3c, a Nyquist graph of these specimens for all reaction conditions is illustrated. In the amplified impedance profile of the EIS, the equivalent series resistance is observed to be approximately 0.69 Ω, which assures a rapid electrochemical reaction process. Figure 3d,e presents the CV and GCD profiles of NiSb/NiTe through various reaction situations, demonstrating the comparatively superior specific capacitance values of sample P3. Excessive microwave heat can lead to surface roughness when the microwave time is raised or the power is boosted, producing agglomerates into lumps and reducing the specific capacitance values of the sample. When the microwave heat is lessened or the duration of the reaction is shortened, the nonuniform superficial morphology leads to voids and cracks, hindered ion transport, and likewise, a degraded capacitance level. Figure 3 shows a dotted line graph consisting of the capacitance values of the NiSb/NiTe electrode under varying densities of current. The nickel backbone is loaded with NiSb for high capacitance and loaded with NiTe to enhance electronic conductivity and facilitate rapid charge transfer. The correlation of the CV plots from the summit current (i) and the frequency of velocity (v) can be deduced from the equation below

https://doi.org/10.1021/acsomega.3c07385
ACS Omega 2024, 9, 2597−2605

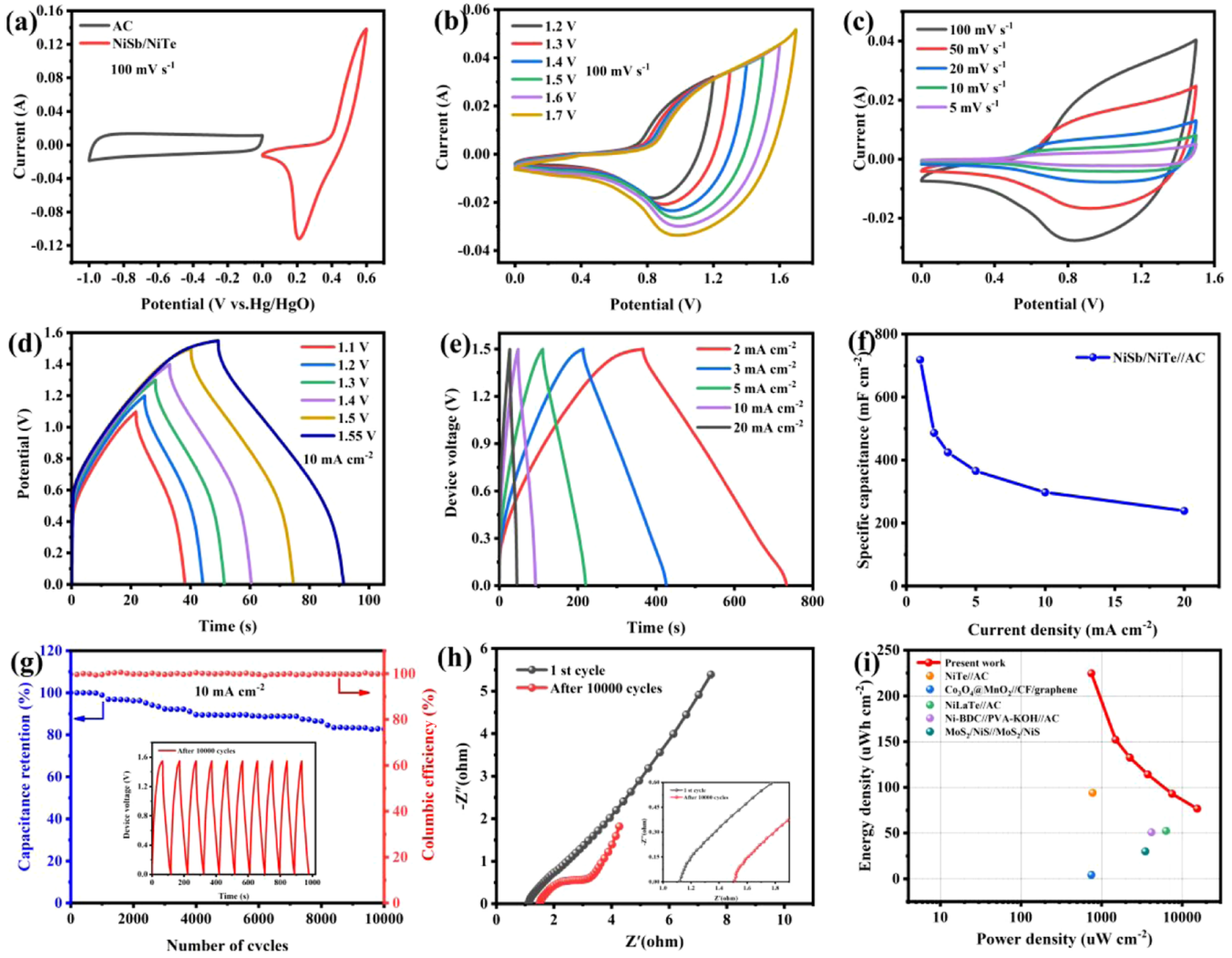

Figure 5. (a) CV profiles of NiSb/NiTe and AC; (b) CV profiles of SC with various voltage gaps; (c) CV graphs of NST//AC at several rates of scanning; (d) GCD profiles of NST//AC at a variety of voltages (10 mA cm^{-2}); (e) GCD profiles of NST//AC with various currents; (f) device's capacitance at variable current densities; (g) variation in cycle stability and Coulombic efficiency; (h) resistance of the device after and before 10,000 cycles; and (i) energy-power density plots of the different devices.

$$i = a \times v^{b} \tag{6}$$

where b represents the fitted slope. The b values from the three peaks are 0.57995 and 0.58506, respectively, in Figure 3g, implying that the electrode stores energy in a pseudocapacitive and battery-type behavior manner, which can be clarified by the formula given below

$$i = k_1 v + k_2 v^{1/2} \tag{7}$$

where $k_1 v$ and $k_2 v^{1/2}$ are the capacitive part of the surface primary control and the capacitive part of the diffusion primary control, respectively. As the sweep rate increases, the percentage contribution of the surface control capacitance also increases, as shown in the histogram in Figure 3h. Due to its high surface capacitance contribution and its fast electrochemical reaction kinetics, it is often considered a battery-type material for storing energy. Generally, the coordinated effect of surface capacitance and the propagation to control capacitance give rise to a large amount of electrical charge storage in NiSb/NiTe materials.[47,48]

The electrochemical performances of the composite electrodes are considered and evaluated in comparison with NiTe. Figure 4 displays these comparisons in terms of CV, CP, and EIS for NiTe and NiSb/NiTe composites, respectively. Here, the NiTe/Ni electrode and NiSb/NiTe/Ni electrode materials were loaded with 1 mg each for the electrochemical comparison test. There is a clear difference in the CV diagrams of both at 50 mV s^{-1}. The constant current charge/discharge plots for NiSb/NiTe reach 1870 F g^{-1} (1 A g^{-1}) compared to the maximum specific capacitance value of 564.1 F g^{-1} (NiTe). The EIS impedance diagram clearly shows that the Rs of composite NiSb/NiTe and single NiTe are 0.59 and 0.78 Ω, respectively. As seen in Figure 4d, NiSb/NiTe displayed long-term cycle stability, remaining above 82% after 30,000 GCD cycles at 10 A g^{-1}. The NiTe nanosheets act as a volume strain buffer between the Ni substrate and NiSb, alleviating the volume inflation that occurs during the discharge/charge of the composite electrode, resulting in excellent cycling stability performances.[46,49−51] The resistances both before and after cycling are comparatively and analytically presented in Figure 4e. After 30,000 GCD test circles, volume expansion and a partially irreversible oxidation reaction of NiSb/NiTe resulted in a deterioration in properties and a change to high internal resistance. Figure 4f shows that the composite has good

https://doi.org/10.1021/acsomega.3c07385
ACS Omega 2024, 9, 2597−2605

multiplicative properties. The NiTe backbone promotes smooth electron transfer throughout the material and effectively alleviates the large bulk strain of NiSb, thereby retarding the structural degradation.[45,52]

3.2.2. Electrochemical Performances of the Asymmetric SC Device (NiSb/NiTe//AC). In order to further explore the behavior of NiSb/NiTe (NST) for device applications, a SC device consisting of NiSb/NiTe and an AC anode was produced. The capacitance value corresponding to NiSb/NiTe at 1.2 mg loading is 1550 F g^{-1} with a voltage window of 0−0.5 V. The capacitance value of the AC is 150 F g^{-1} with a voltage window of −1 to 0 V. The required loading of AC can be calculated as 5.2 mg according to eq 2. Figure 5 shows the electrochemical characteristics of asymmetric SC (ASC). Figure 5a presents the CV curved lines (100 mV s^{-1}) of both the NST and AC electrodes. Figure 5b presents CV curves under different voltages, indicating that a voltage gap of 1.5 V is theoretically possible for ASC. Figure 5c presents CV profiles of NiSb/NiTe//AC at multiple sweep speeds in a 1.5 V window. The GCD curve is presented in Figure 5d in different voltage windows, indicating stable operation at 1.5 V. Figure 5 presents the charge/discharge profile of NST//AC under a 1.5 V voltage window with various current densities. Figure 5f presents the capacitance value for the ASC with various densities of amps. The specific capacitance of the NST//AC device amounts to 718.7 mF cm^{-2} (1 mA cm^{-2}). As is given in Figure 5g, approximately 83% of its initial capacity was kept through 10,000 cycles (10 mA cm^{-2}), reflecting excellent cycling stability. Figure 5h presents the change in impedance of the device with 6 M KOH before and after 10,000 charge/discharge cycles. Figure 5i shows the impressive power and energy density of the ASC compared to other materials ($Ni/Co_3O_4@MnO_2$//carbon fibers/graphene,[53] MoS_2/NiS-7C//MoS_2/NiS-7C,[54] Ni-MOF//AC,[55] NiLaTe//AC,[56] and NiTe//AC[57]), demonstrating that NST//AC has promising applications in energy storage.

4. CONCLUSIONS

In summary, we prepared NiSb/NiTe composite materials by the microwave method. The composites constructed from NiTe and NiSb exhibit excellent electrochemical properties due to the synergistic interaction between them and the full exploitation of the respective capacitive contributions of the two components. It achieves capacitance values up to 1870 F g^{-1} (1 A g^{-1}) and maintains 81.5% of the original capacitance value through 30,000 charge/discharge cycles. Furthermore, the application of NiSb/NiTe electrodes has been demonstrated with assembled devices of NiSb/NiTe//AC ASC, providing a high energy density of 224.6 uW h cm^{-2} with 777 μW cm^{-2} and maintaining a capacitance of 83% after 10,000 cycles. The results pave the way for potential applications of NiSb/NiTe composites in SCs.

■ ASSOCIATED CONTENT

Supporting Information

The Supporting Information is available free of charge at https://pubs.acs.org/doi/10.1021/acsomega.3c07385.

SEM images of NiTe/Ni and NiSb/NiTe/Ni; SEM images of the NiSb/NiTe electrode before and after cycling; and XRD image of the NiSb/NiTe electrode after cycling (PDF)

■ AUTHOR INFORMATION

Corresponding Authors

Feng Feng − *School of Chemistry and Chemical Engineering, Shanxi Datong University, Datong 037009, PR China*; orcid.org/0000-0002-0063-2724; Email: feng-feng64@263.net

Yong Guo − *School of Chemistry and Chemical Engineering, Shanxi Datong University, Datong 037009, PR China*; Email: ybsy_guo@163.com

Zhen Lu − *School of Chemistry and Chemical Engineering, Shanxi Datong University, Datong 037009, PR China*; Email: luzhen0313@aliyun.com

Authors

Haidong Zhao − *School of Chemistry and Chemical Engineering, Shanxi Datong University, Datong 037009, PR China*; orcid.org/0000-0003-0985-0004

Xiaoyan Hu − *School of Chemistry and Chemical Engineering, Shanxi Datong University, Datong 037009, PR China*

Hongjie Kang − *School of Chemistry and Chemical Engineering, Shanxi Datong University, Datong 037009, PR China*

Complete contact information is available at: https://pubs.acs.org/10.1021/acsomega.3c07385

Notes

The authors declare no competing financial interest.

■ ACKNOWLEDGMENTS

This research was funded by the Scientific Activities of Selected Returned Overseas Professionals in Shanxi Province (20220032), the Key Research and Development Project of Shanxi Province (202102090301008), and the Scientific Research Project of Shanxi Datong University (2020CXZ3 and 2020YGZX010).

■ REFERENCES

(1) Poonam; Sharma, K.; Arora, A.; Tripathi, S. K. Review of supercapacitors: Materials and devices. *J. Energy Storage* **2019**, *21*, 801−825.

(2) Tang, Y.; Guo, W.; Zou, R. Nickel-based bimetallic battery-type materials for asymmetric supercapacitors. *Coord. Chem. Rev.* **2022**, *451*, 214242.

(3) Zhao, J.; Tian, Y.; Liu, A.; Song, L.; Zhao, Z. The NiO electrode materials in electrochemical capacitor: A review. *Mater. Sci. Semicond. Process.* **2019**, *96*, 78−90.

(4) Ali, F.; Khalid, N. R.; Tahir, M. B.; Nabi, G.; Shahzad, K.; Ali, A. M.; Kabli, M. R. Capacitive properties of novel Sb-doped Co_3O_4 electrode material synthesized by hydrothermal method. *Ceram. Int.* **2021**, *47* (22), 32210−32217.

(5) Saravanakumar, B.; Jayaseelan, S. S.; Seo, M.-K.; Kim, H.-Y.; Kim, B.-S. $NiCo_2S_4$ nanosheet-decorated 3D, porous Ni film@Ni wire electrode materials for all solid-state asymmetric supercapacitor applications. *Nanoscale* **2017**, *9* (47), 18819−18834.

(6) Lamba, P.; Singh, P.; Singh, P.; Singh, P.; Bharti; Kumar, A.; Gupta, M.; Kumar, Y. Recent advancements in supercapacitors based on different electrode materials: Classifications, synthesis methods and comparative performance. *J. Energy Storage* **2022**, *48*, 103871.

(7) Guan, B.; Li, Y.; Yin, B.; Liu, K.; Wang, D.; Zhang, H.; Cheng, C. Synthesis of hierarchical NiS microflowers for high performance asymmetric supercapacitor. *Chem. Eng. J.* **2017**, *308*, 1165−1173.

(8) Qiu, L.; Yang, W.; Zhao, Q.; Lu, S.; Wang, X.; Zhou, M.; Tao, B.; Xie, Q.; Ruan, Y. NiS Nanoflake-Coated Carbon Nanofiber Electrodes for Supercapacitors. *ACS Appl. Nano Mater.* **2022**, *5* (5), 6192−6200.

(9) Wang, J.; Li, S.; Zhu, Y.; Zhai, S.; Liu, C.; Fu, N.; Hou, S.; Niu, Y.; Luo, J.; Mu, S.; et al. Metal-organic frameworks-derived NiSe@RGO composites for high-performance asymmetric supercapacitors. *J. Electroanal. Chem.* **2022**, *919*, 116548.
(10) Zhou, P.; Fan, L.; Wu, J.; Gong, C.; Zhang, J.; Tu, Y. Facile hydrothermal synthesis of NiTe and its application as positive electrode material for asymmetric supercapacitor. *J. Alloys Compd.* **2016**, *685*, 384−390.
(11) Li, B.; Zheng, M.; Xue, H.; Pang, H. High performance electrochemical capacitor materials focusing on nickel based materials. *Inorg. Chem. Front.* **2016**, *3* (2), 175−202.
(12) Zeng, Z.; Zhao, W.; Yuan, S.; Dong, Y.; Zhu, J.; Jiang, F.; Yang, Y.; Liu, S.; Wang, L.; Ge, P. Advances on Nickel-Based Electrode Materials for Secondary Battery Systems: A Review. *ACS Appl. Energy Mater.* **2022**, *5* (7), 9189−9213.
(13) Verma, S.; Arya, S.; Gupta, V.; Mahajan, S.; Furukawa, H.; Khosla, A. Performance analysis, challenges and future perspectives of nickel based nanostructured electrodes for electrochemical supercapacitors. *J. Mater. Res. Technol.* **2021**, *11*, 564−599.
(14) Chen, Z.; Zhao, Y.; Mo, F.; Huang, Z.; Li, X.; Wang, D.; Liang, G.; Yang, Q.; Chen, A.; Li, Q.; et al. Metal-Tellurium Batteries: A Rising Energy Storage System. *Small Struct.* **2020**, *1* (2), 2000005.
(15) Wang, Z.; Zhang, L. In situ growth of NiTe nanosheet film on nickel foam as electrocatalyst for oxygen evolution reaction. *Electrochem. Commun.* **2018**, *88*, 29−33.
(16) Ye, B.; Xiao, S.; Cao, X.; Chen, J.; Zhou, A.; Zhao, Q.; Huang, W.; Wang, J. Interface engineering for enhancing performance of additive-free NiTe@$NiCoSe_2$ core/shell nanostructure for asymmetric supercapacitors. *J. Power Sources* **2021**, *506*, 230056.
(17) Manikandan, M.; Subramani, K.; Sathish, M.; Dhanuskodi, S. NiTe Nanorods as Electrode Material for High Performance Supercapacitor Applications. *ChemistrySelect.* **2018**, *3* (31), 9034−9040.
(18) Shi, C.; Yang, Q.; Deng, C.; Chen, S.; Hao, Y.; Yan, Y.; Wei, M. 3D hierarchical nanoarrays composed of NiCo-Te multilayer nanoneedles modified with $Co_{1.29}Ni_{1.71}O_4$ for high-performance hybrid supercapacitors. *New J. Chem.* **2021**, *45* (42), 19795−19803.
(19) Wu, B.; Zhang, F.; Nie, Z.; Qian, H.; Liu, P.; He, H.; Wu, J.; Chen, Z.; Chen, S. A high-performance battery-like supercapacitor electrode with a continuous NiTe network skeleton running throughout $Co(OH)_2/Co_9S_8$ nanohybrid. *Electrochim. Acta* **2021**, *365*, 137325.
(20) Hu, Q.; Jiang, X.; He, M.; Zheng, Q.; Lam, K. H.; Lin, D. Core-shell nanostructured $MnO_2@Co_9S_8$ arrays for high-performance supercapacitors. *Electrochim. Acta* **2020**, *338*, 135896.
(21) Fang, L.; Qiu, Y.; Zhai, T.; Wang, F.; Lan, M.; Huang, K.; Jing, Q. Flower-like nanoarchitecture assembled from Bi_2S_3 nanorod/MoS_2 nanosheet heterostructures for high-performance supercapacitor electrodes. *Colloids Surf., A* **2017**, *535*, 41−48.
(22) Mariappan, V. K.; Krishnamoorthy, K.; Pazhamalai, P.; Natarajan, S.; Sahoo, S.; Nardekar, S. S.; Kim, S.-J. Antimonene dendritic nanostructures: Dual-functional material for high-performance energy storage and harvesting devices. *Nano Energy* **2020**, *77*, 105248.
(23) Dong, S.; Li, C.; Yin, L. One-Step In Situ Synthesis of Three-Dimensional NiSb Thin Films as Anode Electrode Material for the Advanced Sodium-Ion Battery. *Eur. J. Inorg. Chem.* **2018**, *2018* (8), 992−998.
(24) Cui, K.; Du, L.; Du, W.; Cui, L.; Zhang, Y.; Chen, W.; Low, C. T. J.; Zai, J. Rational design of hierarchically nanostructured NiTe@Co_xS_y composites for hybrid supercapacitors with impressive rate capability and robust cycling durableness. *J. Colloid Interface Sci.* **2023**, *643*, 292−304.
(25) Yewale, M. A.; Kadam, R. A.; Kaushik, N. K.; Nguyen, L. N.; Nakate, U. T.; Lingamdinne, L. P.; Koduru, J. R.; Auti, P. S.; Vattikuti, S. V. P.; Shin, D. K. Electrochemical supercapacitor performance of $NiCo_2O_4$ nanoballs structured electrodes prepared via hydrothermal route with varying reaction time. *Colloids Surf., A* **2022**, *653*, 129901.
(26) Yang, W.; Guo, H.; Fan, T.; Zhao, X.; Zhang, L.; Guan, Q.; Wu, N.; Cao, Y.; Yang, W. $MoS_2/Ni(OH)_2$ composites derived from in situ grown Ni-MOF coating MoS_2 as electrode materials for supercapacitor and electrochemical sensor. *Colloids Surf., A* **2021**, *615*, 126178.
(27) Usui, H.; Domi, Y.; Uehara, I.; Itoda, Y.; Iwama, E.; Oishi, N.; Nitta, N.; Sakaguchi, H. Cyclability enhancement of CeO_2/Sb_2O_3 composite electrode via ternary Na-storage reactions. *Ceram. Int.* **2022**, *48* (23), 35593−35598.
(28) Jia, R.; Li, L.; Shen, G.; Chen, D. Hierarchical Sb_2S_3/Sn_S2/C heterostructure with improved performance for sodium-ion batteries. *Sci. China Mater.* **2022**, *65* (6), 1443−1452.
(29) Li, G.; Song, M.; Zhang, X.; Sun, Y.; Guo, J. Carbon coated heterojunction $CoSe_2/Sb_2Se_3$ nanospheres for high-efficiency sodium storage. *Dalton Trans.* **2023**, *52* (15), 4973−4979.
(30) Younas, W.; Naveed, M.; Cao, C.; Khalid, S.; Rafai, S.; Wang, Z.; Wu, Y.; Yang, L. Rapid and simplistic microwave assisted method to synthesise cobalt selenide nanosheets; a prospective material for high performance hybrid supercapacitor. *Appl. Surf. Sci.* **2020**, *505*, 144618.
(31) Zhang, Y.; Teng, Y.; Li, Y.; Du, X.; Liu, L.; Wu, Y.; Meng, Y. n.; Hua, Y.; Zhao, X.; Liu, X. Microwave-assisted green synthesis of manganese molybdate nanorods for high-performance supercapacitor. *Ionics* **2019**, *25* (9), 4361−4370.
(32) Zhang, P.; Li, W. Microwave-assisted synthesis of CuO/MnO_2 nanocomposites for supercapacitor application. *Micro Nano Lett.* **2020**, *15* (13), 938−942.
(33) Chen, Z.; Li, Y.; Hu, Z.; Miao, Y.; Sui, Y.; Qi, J.; Wei, F.; Ren, Y.; Zhan, Z.; Liu, J.; et al. In-situ growth of core-shell $NiCo_2O_4$@Ni-Co layered double hydroxides for all-solid-state flexible hybrid supercapacitor. *Colloids Surf., A* **2020**, *607*, 125417.
(34) Li, J.; Jiang, W.; Wang, D. Synthesis of Co_3O_4@CNTs with oxygen vacancies on nickel foam for improved performance of asymmetric supercapacitor electrode. *Colloids Surf., A* **2023**, *658*, 130750.
(35) Ye, B.; Huang, M.; Bao, Q.; Jiang, S.; Ge, J.; Zhao, H.; Fan, L.; Lin, J.; Wu, J. Construction of NiTe/NiSe Composites on Ni Foam for High-Performance Asymmetric Supercapacitor. *ChemElectroChem.* **2018**, *5* (3), 507−514.
(36) Ye, B.; Huang, M.; Jiang, S.; Fan, L.; Lin, J.; Wu, J. In-situ growth of Se-doped NiTe on nickel foam as positive electrode material for high-performance asymmetric supercapacitor. *Mater. Chem. Phys.* **2018**, *211*, 389−398.
(37) Ye, B.; Huang, M.; Fan, L.; Lin, J.; Wu, J. Co ions doped NiTe electrode material for asymmetric supercapacitor application. *J. Alloys Compd.* **2019**, *776*, 993−1001.
(38) Li, J.; Bi, R.; Zhang, T.; Du, L.; Hou, Y.; Wang, F.; Zhang, Z. Microwave one-step controllable synthesis of NiSb materials for high-performance energy storage. *J. Alloys Compd.* **2022**, *909*, 164770.
(39) Kim, S.-I.; Kang, J.-H.; Kim, S.-W.; Jang, J.-H. A new approach to high-performance flexible supercapacitors: Mesoporous three-dimensional Ni-electrodes. *Nano Energy* **2017**, *39*, 639−646.
(40) Chen, H.; Zhou, S.; Wu, L. Porous Nickel Hydroxide-Manganese Dioxide-Reduced Graphene Oxide Ternary Hybrid Spheres as Excellent Supercapacitor Electrode Materials. *ACS Appl. Mater. Interfaces* **2014**, *6* (11), 8621−8630.
(41) Zhao, R.-D.; Cui, D.; Sheng, H.-P.; Gammer, C.; Wu, F.-F.; Xiang, J. Core-shell structured $NiCo_2O_4@Ni(OH)_2$ nanomaterials with high specific capacitance for hybrid capacitors. *Ionics* **2021**, *27* (3), 1369−1376.
(42) Li, P.; Liu, X.; Arif, M.; Yan, H.; Hu, C.; Chen, S.-M.; Liu, X. In situ growth of glucose-intercalated LDHs on $NiCo_2S_4$ hollow nanospheres to enhance energy storage capacity for hybrid supercapacitors. *Colloids Surf., A* **2022**, *644*, 128823.
(43) Xu, X.; Liang, L.; Liu, Q.; Zhang, X.; Zhao, Y.; Qiao, S. In-situ induced sponge-like $NiMoS_4$ nanosheets on self-supported nickel foam skeleton for electrochemical capacitor electrode. *Colloids Surf., A* **2020**, *602*, 125099.

https://doi.org/10.1021/acsomega.3c07385
ACS Omega 2024, 9, 2597−2605

(44) Zhang, Y.; Wang, J.; Yu, L.; Wang, L.; Wan, P.; Wei, H.; Lin, L.; Hussain, S. Ni@$NiCo_2O_4$ core/shells composite as electrode material for supercapacitor. *Ceram. Int.* **2017**, *43* (2), 2057−2062.
(45) Wang, H.; Guo, C.; Ren, X.; Zhang, Y.; Shi, Q.; Bai, Z.; Wang, N. Structurally Stable $Ni(OH)_2$ Composite with Super Long-term Cycling Life for Aqueous High-performance Supercapacitor. *Electroanalysis* **2022**, *34* (8), 1256−1265.
(46) Chen, S.; Wu, B.; Qian, H.; Wu, Z.; Liu, P.; Li, F.; He, H.; Wu, J.; Liu, B. An asymmetric supercapacitor using sandwich-like NiS/NiTe/Ni positive electrode exhibits a super-long cycle life exceeding 200 000 cycles. *J. Power Sources* **2019**, *438*, 227000.
(47) Sivakumar, M.; Muthukutty, B.; Panomsuwan, G.; Veeramani, V.; Jiang, Z.; Maiyalagan, T. Facile synthesis of $NiFe_2O_4$ nanoparticle with carbon nanotube composite electrodes for high-performance asymmetric supercapacitor. *Colloids Surf., A* **2022**, *648*, 129188.
(48) Xu, S.; Li, X.; Yang, Z.; Wang, T.; Jiang, W.; Yang, C.; Wang, S.; Hu, N.; Wei, H.; Zhang, Y. Nanofoaming to Boost the Electrochemical Performance of Ni@$Ni(OH)_2$ Nanowires for Ultrahigh Volumetric Supercapacitors. *ACS Appl. Mater. Interfaces* **2016**, *8* (41), 27868−27876.
(49) Zhai, S.; Jin, K.; Zhou, M.; Fan, Z.; Zhao, H.; Li, X.; Zhao, Y.; Ge, F.; Cai, Z. A novel high performance flexible supercapacitor based on porous carbonized cotton/ZnO nanoparticle/CuS micro-sphere. *Colloids Surf., A* **2020**, *584*, 124025.
(50) Pillai, A. S.; Rajagopalan, R.; Amruthalakshmi, A.; Joseph, J.; Ajay, A.; Shakir, I.; Nair, S. V.; Balakrishnan, A. Mesoscopic architectures of $Co(OH)_2$ spheres with an extended array of microporous threads as pseudocapacitor electrode materials. *Colloids Surf., A* **2015**, *470*, 280−289.
(51) Mi, X.; Tingwu, Z.; Xu, N.; Tianrui, W.; Meilian, Z.; Yupeng, S. Construction of hierarchical $ZnCo_2O_4$@CoSe core-shell nanosheets on Ni foam for high-performance supercapacitor. *Ionics* **2021**, *27* (12), 5251−5261.
(52) Mordina, B.; Kumar, R.; Neeraj, N. S.; Srivastava, A. K.; Setua, D. K.; Sharma, A. Binder free high performance hybrid supercapacitor device based on nickel ferrite nanoparticles. *J. Energy Storage* **2020**, *31*, 101677.
(53) Niu, X.; Zhu, G.; Yin, Z.; Dai, Z.; Hou, X.; Shao, J.; Huang, W.; Zhang, Y.; Dong, X. Fiber-based all-solid-state asymmetric supercapacitors based on Co_3O_4@MnO_2 core/shell nanowire arrays. *J. Mater. Chem. A* **2017**, *5* (44), 22939−22944.
(54) Wang, H.; Tian, L.; Zhao, X.; Ali, M.; Yin, K.; Xing, Z. In situ growth MoS_2/NiS composites on Ni foam as electrode materials for supercapacitors. *Mater. Today Commun.* **2023**, *34*, 105041.
(55) Yang, C.; Li, X.; Yu, L.; Liu, X.; Yang, J.; Wei, M. A new promising Ni-MOF superstructure for high-performance supercapacitors. *Chem. Commun.* **2020**, *56* (12), 1803−1806.
(56) Bhol, P.; Jagdale, P. B.; Barman, N.; Thapa, R.; Saxena, M.; Samal, A. K. Design and fabrication of nickel lanthanum telluride microfibers for redox additive electrolyte-based flexible solid-state hybrid supercapacitor. *J. Energy Storage* **2023**, *65*, 107286.
(57) Zhang, T.; Li, J.; Bi, R.; Song, J.; Du, L.; Li, T.; Zhang, H.; Guo, Q.; Luo, J. One-step microwave synthesis of in situ grown NiTe nanosheets for solid-state asymmetric supercapacitors and oxygen evolution reaction. *J. Alloys Compd.* **2022**, *909*, 164786.

https://doi.org/10.1021/acsomega.3c07385
ACS Omega 2024, 9, 2597−2605